JOURNAL OF SOLID STATE CHEMISTRY 104, 319–327 (1993)

Crystal Structure of the Magnetoplumbite-Type Oxide $NaFe_3V_9O_{19}$

Y. KANKE,† F. IZUMI, Y. MORII,* S. FUNAHASHI,* AND K. KATO

*National Institute for Research in Inorganic Materials, 1-1 Namiki, Tsukuba, Ibaraki 305, Japan, and *Department of Physics, Japan Atomic Energy Research Institute, Tokai-mura, Naka-gun, Ibaraki 319-11, Japan*

Received August 3, 1992; accepted October 13, 1992

The crystal structure of $NaFe_3V_9O_{19}$ (hexagonal, $P6_3/mmc$, a = 5.8388(1), c = 22.8017(3) Å) was determined by Rietveld refinements of both neutron and X-ray powder diffraction data. $NaFe_3V_9O_{19}$ crystallizes in the magnetoplumbite-type structure ($AM_{12}O_{19}$: A = Na, M = Fe and V). The $M(3)$ site, which corresponds to the tetrahedral site of the spinel structure, is occupied exclusively by Fe. The rest of the Fe cations are not concentrated at any particular $M(n)$ sites. Structural details and cation distribution in $NaFe_3V_9O_{19}$ are discussed in comparison with those in related compounds.

Introduction

Magnetoplumbite ferrites (hexagonal, $P6_3/mmc$), $BaFe_{12}O_{19}$ (*1*) and $LaFe_{12}O_{19}$ (*2*), show uniaxial ferrimagnetisms (*3–9*) with the easy axes of magnetization parallel to [001]. Their magnetic structures have been described on the basis of localized *d*-electron models (*3–9*). NaV_6O_{11} and SrV_6O_{11} (hexagonal, $P6_3/mmc$) (*10*) have been revealed to be structurally related to magnetoplumbite. NaV_6O_{11} shows spontaneous magnetization (T_c = 64.2 K) with the easy axis of magnetization parallel to [001] (*11*). We indicated that itinerant *d*-electrons play important roles in its magnetism (*11*), in contrast to $BaFe_{12}O_{19}$ and $LaFe_{12}O_{19}$ (*3–9*). T cations in $SrT_xV_{6-x}O_{11}$ (T = Ti, Cr, and Fe) are not concentrated in particular V sites but distributed randomly, which suggests that SrV_6O_{11} contains itinerant *d*-electrons also (*12*).

$NaFe_3V_9O_{19}$ (*13*) is isomorphous with magnetoplumbite. It shows spontaneous magnetization ($T_c \approx 240$ K) with the easy axis of magnetization parallel to [001] (*13*). Whether or not $NaFe_3V_9O_{19}$ contains itinerant *d*-electrons is of great interest in connection with its magnetic and electric properties. We have now determined the crystal structure of $NaFe_3V_9O_{19}$ by Rietveld refinements of both neutron and X-ray diffraction data. In this paper, structural details and cation distribution in $NaFe_3V_9O_{19}$ are discussed in comparison with those in related compounds.

Experiment and Refinement

V_2O_3 was obtained by reducing V_2O_5 (99.9%) in hydrogen at 1073 K. V_2O_4 was prepared by heating an equimolar mixture of V_2O_5 and V_2O_3 in a sealed silica tube at 1273 K for 3 days. Another starting material, β-$NaFeO_2$, was prepared by heating an equimolar mixture of Na_2CO_3 (99.9%) and Fe_2O_3 (99.9%) at 1073 K for 1 day with an intermediate grinding.

The starting materials, β-$NaFeO_2$, Fe_2O_3, V_2O_4, and V_2O_3, were mixed in a 1 : 1 : 0.5 : 4 molar ratio. About 10 g of the mixture was placed in a platinum capsule, sealed in an

† To whom correspondence should be addressed.

0022-4596/93 $5.00

TABLE I

STRUCTURAL PARAMETERS IN $NaFe_3V_9O_{19}$

Hexagonal, $P6_3/mmc$, $Z = 2$, $a = 5.83884(7)$,[a] $c = 22.8017(3)$[a] Å
($a = 5.8380(2)$,[b] $c = 22.8020(6)$[b] Å).

Sites	Positions[c]	g(Fe(n))[d]	x	y	z	B/Å^2
$M(1)$	2a	0.07(2)[a]	0	0	0	0.44(15)[b]
$M(2)$	2b	0.13(2)[a]	0	0	$\frac{1}{4}$	0.53(15)[b]
$M(3)$	4f	1[e]	$\frac{1}{3}$	$\frac{2}{3}$	0.5281(4)[a]	0.65(13)[a]
$M(4)$	4f	0.185(15)[a]	$\frac{1}{3}$	$\frac{2}{3}$	0.6933(2)[b]	0.51(11)[b]
$M(5)$	12k	0.071[f]	0.1699(4)[b]	$2x$	0.10993(10)[b]	0.41(6)[b]
O(1)	4e		0	0	0.1579(6)[a]	0.6(2)[a]
O(2)	4f		$\frac{1}{3}$	$\frac{2}{3}$	0.0565(5)[a]	0.6(2)[a]
O(3)	6h		0.1779(10)[a]	$2x$	$\frac{3}{4}$	0.68(17)[a]
O(4)	12k		0.1511(6)[a]	$2x$	0.5551(3)[a]	0.56(13)[a]
O(5)	12k		0.4996(6)[a]	$2x$	0.1508(3)[a]	0.51(12)[a]
Na	2c		$\frac{1}{3}$	$\frac{2}{3}$	$\frac{1}{4}$	3.4(8)[a]

$R_{wp} = 7.38\%$, $R_e = 3.52\%$, $R_p = 5.64\%$, $R_I = 6.37\%$ (neutron diffraction)
$R_{wp} = 8.55\%$, $R_e = 4.11\%$, $R_p = 6.49\%$, $R_I = 4.17\%$ (X-ray diffraction)

Note. Estimated standard deviations given in parentheses refer to the least significant digit(s).
[a] Refined using the neutron powder diffraction data.
[b] Refined using the X-ray powder diffraction data.
[c] Multiplicity m and Wyckoff letter. Number of atoms per unit cell = $m \times g$.
[d] Occupancy of Fe(n) at $M(n)$ sites. g(V(n)) = 1 − g(Fe(n)).
[e] *Fixed (see text).*
[f] Constrained as follows: $g(\text{Fe}(5)) = \{1 - g(\text{Fe}(1)) - g(\text{Fe}(2)) - 2g(\text{Fe}(4))\}/6$.

evacuated silica tube, and then heated at 993 K for 1 day. After cooling to room temperature, the product was ground and identified by X-ray powder diffraction with graphite-monochromatized Cu$K\alpha$ radiation. This procedure was repeated until its X-ray powder pattern no longer changed. Three heating runs (1 + 3 + 3 days) were required to obtain pure $NaFe_3V_9O_{19}$. Its chemical composition was confirmed to be Na : Fe : V =

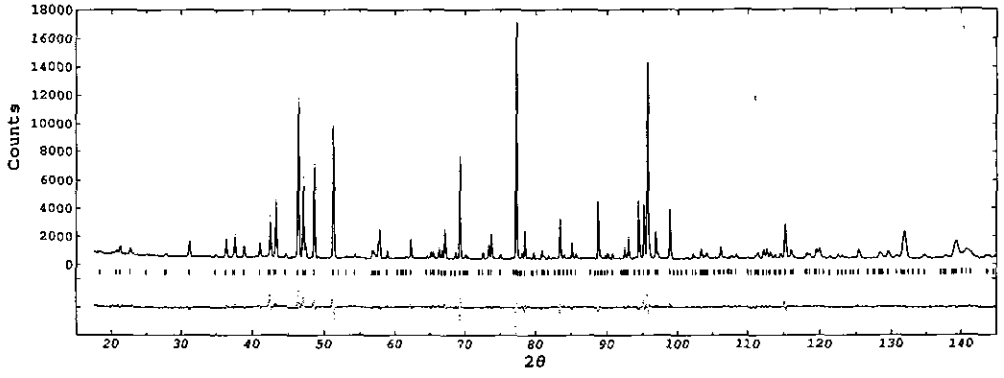

FIG. 1. Observed (+ marks), calculated (upper solid line), and difference (lower solid line) neutron powder diffraction patterns of $NaFe_3V_9O_{19}$. Background has been subtracted to show net intensities. Vertical marks indicate the positions of possible Bragg reflections ($\lambda = 1.823$ Å).

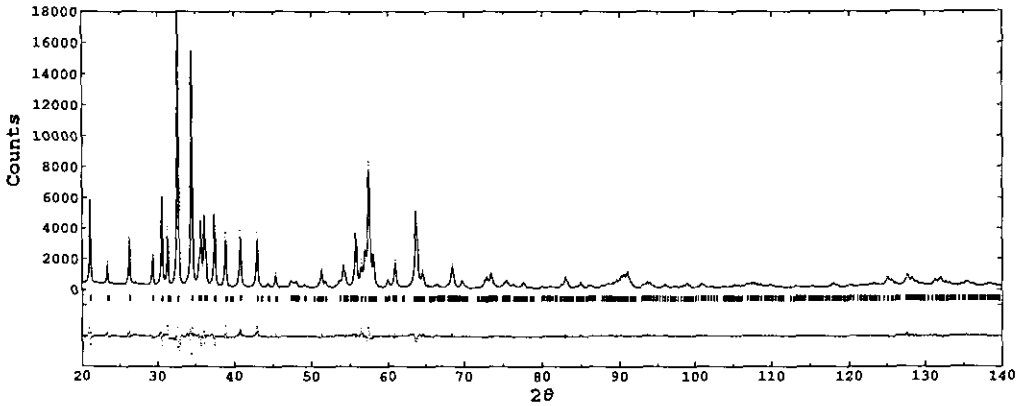

FIG. 2. Observed, calculated, and difference X-ray powder diffraction patterns of $NaFe_3V_9O_{19}$ (Cu$K\alpha$).

1:2:8(2):9.0(4) by X-ray microanalysis (*13*).

X-ray powder diffraction data were collected at room temperature on a Rigaku RAD-2B diffractometer (graphite-monochromatized Cu$K\alpha$) with a 2θ step width of 0.04°. To minimize preferred orientation, the specimen was dispersed in an acetone solution of a cellulose resin, and the solid obtained by evaporation was ground to a powder, which was mounted on a glass holder.

Neutron powder diffraction data were collected at room temperature on the HRPD angle-dispersive type diffractometer installed at the JRR-3 reactor at JAERI (*14*). The incident neutron beam was monochromatized to give a wavelength of 1.823 Å using the 331 reflection of Ge. The

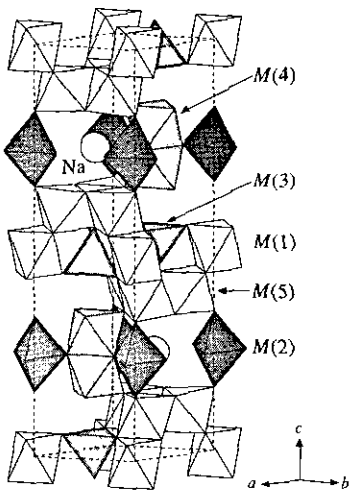

FIG. 3. Crystal structure of $NaFe_3V_9O_{19}$ drawn with ATOMS (Shape Software). Broken lines represent unit-cell edges. Fe and V cations are located within coordination polyhedra. $M(1)$ octahedra and $M(3)$ tetrahedra form S-blocks. The $M(2)$ site is a trigonal bipyramidal position. $M(4)$ octahedra form face-shared dimers. $M(5)$ octahedra form edge-shared networks.

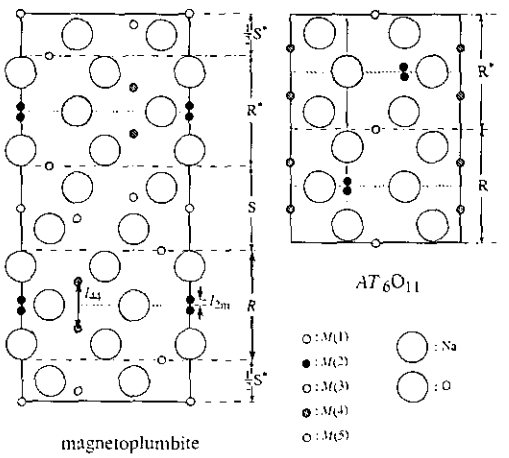

FIG. 4. [110] sectional views of the magnetoplumbite-type and AT_6O_{11} structures. S and R represent the spinel and R blocks. Vertical lines indicate threefold axes. Broken lines denote mirror planes vertical to [001].

TABLE II

LATTICE PARAMETERS, THICKNESSES OF THE R AND S BLOCKS, AND INTERATOMIC DISTANCES IN $NaFe_3V_9O_{19}$ AND RELATED OXIDES (UNIT: Å)

		$NaFe_3V_9O_{19}$	$SrFe_{12}O_{19}$	$SrFe_{12}O_{19}$	$BaFe_{12}O_{19}$	$BaFe_{12}O_{19}$	$CaAl_{12}O_{19}$	$SrAl_{12}O_{19}$
a		5.83884(7)	5.8844(6)	5.8836(1)	5.893	5.8920(1)	5.5587(1)	5.5666(2)
c		22.8017(3)	23.050(3)	23.0376(9)	23.194	23.183(1)	21.8929(3)	22.0018(8)
R		6.389(3)	6.486(3)	6.4888(3)	6.573(3)	6.5724(3)	6.1677(3)	6.2335(9)
S		5.012(3)	5.039(3)	5.0300(3)	5.024(3)	5.0191(3)	4.7788(3)	4.7674(9)
$M(1)$–O(4^{i})	(×6)	1.979(7)	2.005(2)	2.001(2)	1.995(6)	2.000(2)	1.879	1.876(2)
$M(2)$–O(1)	(×2)	2.099(14)	2.171(7)	2.157(4)	2.170(11)	2.128(3)	2.041	2.025(4)
			2.365(7)	2.384(4)	2.472(11)	2.468(3)	2.378	2.450(4)
$M(2)$–O(3^{ii})	(×3)	1.799(10)	1.854(1)	1.858(3)	1.886(10)	1.867(2)	1.751	1.765(3)
Mean $M(2)$–O		1.919	2.020	2.023	2.060	2.039	1.934	1.954
$M(3)$–O(2^{i})	(×1)	1.929(15)	1.899(3)	1.901(4)	1.897(11)	1.894(3)	1.810	1.813(4)
$M(3)$–O(4)	(×3)	1.943(7)	1.896(2)	1.896(2)	1.936(9)	1.894(2)	1.795	1.798(2)
Mean $M(3)$–O		1.940	1.897	1.897	1.926	1.894	1.799	1.802
$M(4)$–O(3)	(×3)	2.036(8)	2.060(2)	2.058(2)	2.060(7)	2.073(2)	1.954	1.963(3)
$M(4)$–O(5^{iii})	(×3)	1.947(7)	1.976(2)	1.963(2)	1.975(8)	1.969(2)	1.876	1.877(2)
Mean $M(4)$–O		1.992	2.018	2.011	2.018	2.021	1.915	1.920
$M(5)$–O(1)	(×1)	2.038(8)	1.978(2)	1.977(2)	1.977(5)	1.985(2)	1.843	1.847(2)
$M(5)$–O(2)	(×1)	2.053(8)	2.089(2)	2.085(2)	2.091(6)	2.092(2)	1.986	1.985(2)
$M(5)$–O(4^{iv})	(×2)	2.056(8)	2.113(2)	2.112(2)	2.106(4)	2.114(3)	1.999	1.999(2)
$M(5)$–O(5^{v})	(×2)	1.910(7)	1.919(2)	1.923(3)	1.928(5)	1.932(3)	1.806	1.813(3)
Mean $M(5)$–O		2.004	2.022	2.022	2.023	2.028	1.907	1.909
Na, Ba–O(3^{iv})	(×6)	2.922(8)	2.946(1)	2.946(3)	2.952(1)	2.950(2)	2.783	2.787(3)
Na, Ba–O(5)	(×6)	2.818(7)	2.820(2)	2.821(2)	2.865(6)	2.868(2)	2.712	2.746(2)
Mean Na, Ba–O		2.870	2.883	2.884	2.909	2.909	2.748	2.767
$2l_{2m}$		0	0.194(10)	0.227(4)	0.312(20)	0.340(1)	0.338	0.424(4)
l_{44}		2.587(6)	2.725(3)	2.7226(7)	2.778(1)	2.768(1)	2.582	2.618(2)
Ref.		This work	(18)	(21)	(1)	(17)	(19)	(21)

HRPD has a bank of 64 counters placed in 2.5° intervals and Söller collimators of 6′ divergence. A scan moves each one of the multicounters at a step width of 0.05° over a relatively small portion of the whole scan range. About 6.4 g of the sample was contained in a cylindrical vanadium cell, which was rotated on its axis during data collection.

Both neutron diffraction data ($17.5° \leq 2\theta \leq 157.5°$) and X-ray diffraction data ($20.0° \leq 2\theta \leq 140.0°$) were analyzed by the Rietveld method with RIETAN (*15*). The coherent scattering lengths, b, used for refinement of the neutron diffraction data were 3.63 fm (Na), 9.54 fm (Fe), −0.3824 fm (V), and 5.803 fm (O) (*16*).

Rietveld refinements were started using the following crystallographic information: space group $P6_3/mmc$ (No. 194), lattice parameters determined by X-ray powder diffraction, and fractional coordinates of $BaFe_{12}O_{19}$ (*1*). Eleven sites are contained in its asymmetric unit: $M(1)$–$M(5)$, O(1)–O(5), and Na, where M is Fe and/or V (cf. Table I). Isotropic thermal parameters, B, were assigned for all the atoms. The occupancies, g, of the O and Na sites were fixed at 1. On the other hand, the occupancies of the five M sites were refined by imposing constraints that the total occupancies, $g(\mathrm{Fe}(n)) + g(\mathrm{V}(n))$, for all the M sites are 1 and that $g(\mathrm{Fe}(5))$ is equal to $\{3 - g(\mathrm{Fe}(1)) - g(\mathrm{Fe}(2)) - 2g(\mathrm{Fe}(3)) - 2g(\mathrm{Fe}(4))\}/6$.

At the initial stage, the lattice parameters, the occupancies of Fe atoms in all the $M(n)$ sites, and all the structural parameters of Na and O atoms were refined using the neutron diffraction data, while the positional and thermal parameters of Fe and V atoms were fixed. At the second stage, the lattice parameters and the positional and thermal parameters of the Fe and V atoms were refined using X-ray diffraction data, while the remaining struc-

TABLE II—*Continued*

		$PbAl_{12}O_{19}$	$SrGa_{12}O_{19}$	NaV_6O_{11}	SrV_6O_{11}	$BaTi_2Fe_4O_{11}$	$BaSn_2Fe_4O_{11}$	$BaSn_2Fe_4O_{11}$
a		5.5711(3)	5.7929(1)	5.7123(1)	5.7716(1)	5.8470(2)	5.9624(5)	5.969(2)
c		22.045(2)	22.8123(7)	13.0974(4)	13.0793(5)	13.6116(9)	13.7468(14)	13.764(3)
R		6.261(3)	6.4176(3)	6.5487(2)	6.5397(3)	6.8058(5)	6.8734(7)	6.882(2)
S		4.762(3)	4.9886(3)					
$M(1)$–O(4^{i})	(×6)	1.879(6)	1.967(7)					
$M(2)$–O(1)	(×2)	2.044(14)	2.128(5)	2.086(1)	2.11(1)	2.098(14)	2.044(10)	2.028(11)
		2.458(14)	2.459(5)			2.583(14)	2.603(10)	2.613(11)
$M(2)$–O(3^{iii})	(×3)	1.771(11)	1.831(4)	1.7869(6)	1.832(6)	1.867(5)	1.907(5)	1.909(8)
Mean $M(2)$–O		1.963	2.016	1.907	1.94	2.056	2.074	2.074
$M(3)$–O(2^{i})	(×1)	1.812(10)	1.901(4)					
$M(3)$–O(4)	(×3)	1.804(7)	1.870(2)					
Mean $M(3)$–O		1.806	1.878					
$M(4)$–O(3)	(×3)	1.966(8)	2.047(3)	2.0210(2)	2.026(1)	2.105(8)	2.163(4)	2.142(6)
$M(4)$–O(5^{iii})	(×3)	1.880(7)	1.944(3)	1.9024(3)	1.949(2)	1.933(7)	1.998(5)	2.018(7)
Mean $M(4)$–O		1.923	1.996	1.9617	1.988	2.019	2.081	2.080
$M(5)$–O(1)	(×1)	1.847(6)	1.921(2)	2.0327(6)	2.029(6)	1.997(4)	2.052(3)	2.055(5)
$M(5)$–O(2)	(×1)	1.987(6)	2.064(2)	2.0327(6)	2.029(6)	1.997(4)	2.052(3)	2.055(5)
$M(5)$–O(4^{iv})	(×2)	1.992(7)	2.082(2)	1.9410(4)	1.945(3)	1.997(4)	2.010(3)	2.007(2)
$M(5)$–O(5^{v})	(×2)	1.811(7)	1.885(3)	1.9410(4)	1.945(3)	1.997(4)	2.010(3)	2.007(2)
Mean $M(5)$–O		1.907	1.987	1.9716	1.973	1.997	2.024	2.023
Na, Ba–O(3^{iv})	(×6)	2.790(9)	2.900(4)	2.8595(5)	2.891(4)	2.928(4)	2.987(4)	2.989(1)
Na, Ba–O(5)	(×6)	2.772(5)	2.803(3)	2.7436(5)	2.697(3)	2.828(4)	2.842(4)	2.844(5)
Mean Na, Ba–O		2.781	2.852	2.8016	2.794	2.878	2.915	2.917
$2l_{2m}$		0.414(16)	0.330(3)	0	0	0.485(24)	0.559(17)	0.586(6)
l_{44}		2.640(6)	2.741(1)	2.6840(4)	2.721(3)	2.904(22)	3.002(8)	2.937(18)
Ref.		(*20*)	(*21*)	(*10*)	(*10*)	(*24*)	(*24*)	(*25*)

Note. Symmetry codes: (i) $x, y, \frac{1}{2} - z$; (ii) $-x, -y, 1 - z$; (iii) $1 - x, y - x, \frac{1}{2} + z$; (iv) $y, x, -\frac{1}{2} + z$; (v) $1 - y, 1 - x, z$; (vi) $x, y, \frac{3}{2} - z$. These codes are not applicable to AT_6O_{11}-type compounds.

tural parameters were fixed at the values obtained in the initial stage. At the third stage, the parameters refined in the first stage were re-refined using the neutron diffraction data, with the remaining parameters fixed at the values obtained in the second stage. The occupancy, $g(V(3))$, converged to a negative value, $-0.04(2)$, showing that the $M(3)$ site, which corresponds to the tetrahedral site of the spinel structure, is occupied exclusively by Fe. Then refinements using the X-ray and neutron diffraction data were repeated alternately in the same way as above with $g(V(3))$ fixed at zero until variable structural parameters were virtually unchanged except for the lattice parameters.

The $M(2)$ site is trigonal bipyramidal and generally shifts from an ideal 2b position $(0, 0, \frac{1}{4})$ to a 4e position $(0, 0, \frac{1}{4} \pm \Delta z)$ in magnetoplumbite phases (*1, 17–21*). The validity of the model with $M(2)$ at the 4e position was checked using the X-ray diffraction data. However, the resulting shift (Δz) was essentially zero (0.00008 ± 0.08), and changes in R factors were negligible ($\Delta R_{wp} = +0.01\%$, $\Delta R_p = +0.01\%$, $\Delta R_I = -0.08\%$). Thus, the $M(2)$ atom proved to be at the ideal 2b position.

The final profile fit and difference patterns of $NaFe_3V_9O_{19}$ are shown in Fig. 1 (neutron diffraction) and Fig. 2 (X-ray diffraction). Final structural parameters are listed in Table I.

Discussion

Figure 3 shows the configurations of coordination polyhedra and Na^+ cations in $NaFe_3V_9O_{19}$. The $M(1)$ and the $M(3)$ sites correspond to octahedral and tetrahedral sites in the spinel structure. The $M(2)$ site, located in the mirror plane perpendicular to [001], is a trigonal bipyramidal site. Two $M(4)$ octahedra adjoin each other across this mirror plane and form a face-shared dimer. The $M(5)$ octahedra form edge-shared net-

works parallel to (001). In $NaFe_3V_9O_{19}$, every polyhedron shares corners with adjacent nonequivalent polyhedra. The magnetoplumbite-type structure is usually described as an alternating stack of S-blocks (spinel blocks) and R-blocks (*22*). The S-block contains the polyhedra of $M(1)$ and $M(3)$, and the R-block those of $M(2)$ and $M(4)$. In what follows, the thicknesses of the S- and R-blocks will be denoted as R and S. The layer of $M(5)$ forms the boundary shared by the two blocks. On the other hand, the AT_6O_{11} structure consists exclusively of R-blocks. As Fig. 4 shows, the unit cells of the magnetoplumbite-type and AT_6O_{11} structures are expressed as $(RS)_2$ and R_2, respectively.

Table II shows lattice parameters, R, S, and interatomic distances in $NaFe_3V_9O_{19}$ and its related compounds. The $M(2)$ sites of the V-free phases deviate from the mirror plane and split into a pair of equivalent positions. The $M(2)$ cation occupies one of the paired positions randomly. Taking into account the differences in the crystal structures and kinds of M, we classify these phases except for $SrGa_{12}O_{19}$ into the following three groups: (i) $NaFe_3V_9O_{19}$, $SrFe_{12}O_{19}$, and $BaFe_{12}O_{19}$, (ii) $CaAl_{12}O_{19}$, $SrAl_{12}O_{19}$, and $PbAl_{12}O_{19}$, and (iii) NaV_6O_{11}, SrV_6O_{11}, $BaTi_2Fe_4O_{11}$, and $BaSn_2Fe_4O_{11}$. Whereas S and the shorter $M(2)$–O(1) and mean $M(n)$–O distances ($n \neq 2$) are almost constant within each group, R and the longer $M(2)$–O(1), $M(2)$–$M(2)$, and $M(4)$–$M(4)$ distances change considerably from compound to compound. The $M(4)$–$M(4)$ distance (hereafter denoted as l_{44}) and R are shown as functions of the $M(2)$–mirror plane distance (hereafter denoted as l_{2m}) in Figs. 5 and 6, respectively. We have already pointed out that the differences in both l_{44} and R are attributable merely to those in l_{2m} among the group (iii) compounds (*10*). That is, both lines for group (iii) in Figs. 5 and 6 are linear with slopes approximately equal to 1. These figures show that the same correlation exists also in group (i), and that $NaFe_3V_9O_{19}$ really belongs to this ferrite group. The structure

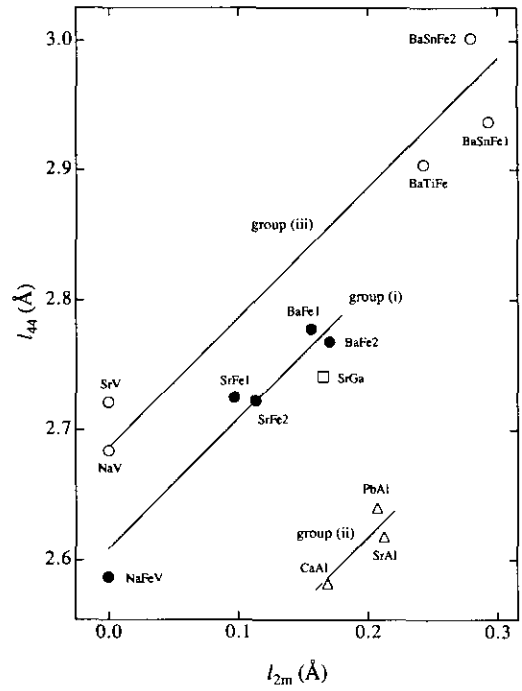

FIG. 5. $M(4)$–$M(4)$ distance (l_{44}) versus $M(2)$–mirror plane distance (l_{2m}) in magnetoplumbite-type and AT_6O_{11} phases. The slopes of straight lines are fixed at 1. Group (i): NaFeV: $NaFe_3V_9O_{19}$ (this work); SrFe1: $SrFe_{12}O_{19}$ (*18*); SrFe2: $SrFe_{12}O_{19}$ (*21*); BaFe1: $BaFe_{12}O_{19}$ (*1*); BaFe2: $BaFe_{12}O_{19}$ (*17*). Group (ii): CaAl: $CaAl_{12}O_{19}$ (*19*); SrAl: $SrAl_{12}O_{19}$ (*21*); PbAl: $PbAl_{12}O_{19}$ (*20*). Group (iii): NaV: NaV_6O_{11} (*10*); SrV: SrV_6O_{11} (*10*); BaTiFe: $BaTi_2Fe_4O_{11}$ (*24*); BaSnFe1: $BaSn_2Fe_4O_{11}$ (*24*); BaSnFe2: $BaSn_2Fe_4O_{11}$ (*25*). SrGa: $SrGa_{12}O_{19}$ (*21*).

of the unit composed of the network of $M(5)$ octahedra and the adjacent $M(4)$ layer as well as the structure of the S-block are nearly the same throughout group (i) compounds.

If we extrapolate the lines in Figs. 5 and 6 to the zero point of the abscissa, we can obtain ideal l_{44} and R distances for each compound group that are not affected by the splitting of the $M(3)$ sites. Group (ii) has by far the smallest l_{44} and R values of the three groups, which reflects the small ionic radius of the Al^{3+} cation. However, the order, group (iii) > group (i), is in conflict with the order of ionic radii of the M cations

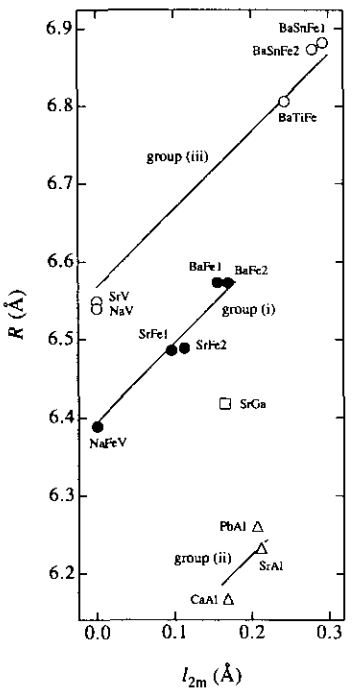

FIG. 6. Thickness of the R block (R) versus $M(2)$–mirror plane distance (l_{2m}) for magnetoplumbite-type and AT_6O_{11}-type phases. The slopes of straight lines are fixed at 1.

(*23*). This can be attributed to the different strengths of electrostatic repulsions between the $M(4)$ cations in face-shared octahedra. Such repulsions are stronger in group (iii) than in group (i) because the $M(4)$ sites in the group (iii) compounds are occupied to a considerable extent by tetravalent cations (*10, 12, 24, 25*) while $M(4)$ cations in the group (i) compounds are generally trivalent. It is rather noticeable that $NaFe_3V_9O_{19}$ belongs to group (i) in spite of the inclusion of tetravalent cations, V^{4+}.

Madelung energies of $NaFe_3V_9O_{19}$ were calculated by the Fourier method for several cation distributions on the assumption that all Fe cations are trivalent (Table III). The results suggest that the $M(2)$ and $M(4)$ sites prefer cations with higher oxidation states while the $M(1)$ and $M(3)$ sites prefer cations with lower ones. Both Fe^{2+} and Fe^{3+} cations are well known to enter tetrahedral or trigonal bipyramidal sites (*26–31*). However, V^{3+} cations do not prefer to occupy them. Tetrahedrally coordinated V^{3+} has not been reported. Tetrahedrally coordinated V^{4+} exists only in $Sr_2V^{IV}O_4$ (*32*). V^{4+} can be situated in five-coordinated sites (*33, 34*). Thus, in $NaFe_3V_9O_{19}$ (which becomes either $NaFe^{III}_3V^{III}_8V^{IV}O_{19}$ or $NaFe^{II}V^{III}_5V^{IV}_4O_{19}$ on perfect disproportionation), Fe cations are expected to occupy the $M(1)$, $M(2)$, or $M(3)$ sites, and V cations the $M(2)$ or $M(4)$ sites. Table I shows, however, that the $M(n)$ sites do not really accommodate cations as expected above. Though the $M(3)$ site is fully occupied by Fe, the rest of Fe cations are not concentrated at any particular $M(n)$ sites. Moreover, $g(Fe(1))$ is smaller than $g(Fe(4))$ in conflict with the above expectation. On the other hand, Fe^{2+} cations in $LaFe^{II}Fe^{III}_{11}O_{19}$ are located in the $M(1)$ sites (*3, 6–9*), and more than 90% of Zn^{2+} cations in $LaZn^{II}Fe^{III}_{11}O_{19}$ are concentrated in the $M(3)$ sites (*35*). The cations in $LaFe_{12}O_{19}$ and $LaZnFe_{11}O_{19}$ are distributed in such a way as to achieve electrostatic stability and to obey the order of preference for the tetrahedral site: $Zn^{2+} > Fe^{3+} > Fe^{2+}$.

The 3*d* orbitals of cations in the first transition series contract with increasing atomic number (*36*). Numbers of 3*d* electrons are small for V^{3+} ($3d^2$) and V^{4+} ($3d^1$) cations but relatively large for Fe^{2+} ($3d^6$) and Fe^{3+} ($3d^5$) cations. Therefore, electrostatic repulsions among the 3*d* electrons within an atom are weak for V^{3+} and V^{4+} cations but strong for Fe^{2+} and Fe^{3+} cations. Thus, the 3*d* electrons in V^{III}–V^{IV} oxides are expected to be delocalized while those in Fe^{II}–Fe^{III} oxides are expected to be localized. Indeed, $LiV^{III}V^{IV}O_4$ (normal spinel) behaves as a metallic conductor independently of temperature (*37*) whereas $Fe^{II}Fe^{III}_2O_4$ (inverse spinel) shows a metal–insulator transition at around 120 K (*38*). The octahedral site in LiV_2O_4 accommodates equal amounts of V^{3+} and V^{4+} cations. The corresponding site in Fe_3O_4 also contains equal amounts of Fe^{2+} and Fe^{3+} cations, but they separate into Fe^{2+} and Fe^{3+} sites below the transition

TABLE III

ELECTROSTATIC POTENTIALS (ϕ) OF THE $M(n)$ SITES AND MADELUNG ENERGIES (E_M) FOR FIVE TYPICAL CHARGE DISTRIBUTIONS IN $NaFe_3V_9O_{19}$

$M(1)$	$+\frac{37}{12}$	+4	+3	+3	+3	+3
$M(2)$	$+\frac{37}{12}$	+3	+4	+3	+3	+3
$M(3)$	$+\frac{37}{12}$	+3	+3	+3.5	+3	+3
$M(4)$	$+\frac{37}{12}$	+3	+3	+3	+3.5	+3
$M(5)$	$+\frac{37}{12}$	+3	+3	+3	+3	$\frac{19}{8}$
$\phi(M(1))$/V	−28.93	−32.71	−31.03	−26.35	−30.64	−28.24
$\phi(M(2))$/V	−44.99	−46.39	−48.07	−46.32	−42.34	−44.69
$\phi(M(3))$/V	−27.64	−24.96	−29.57	−28.45	−29.04	−27.03
$\phi(M(4))$/V	−42.22	−43.36	−39.70	−43.15	−42.98	−41.88
$\phi(M(5))$/V	−33.71	−32.80	−33.90	−32.98	−33.72	−34.08
E_M/MJ · mol^{-1}	−9.082	−9.052	−9.176	−9.030	−9.145	−9.076

temperature (*26, 39*). The disordered distribution of Fe cations, coupled with the above discussion, suggests the possible existence of itinerant 3d electrons in $NaFe_3V_9O_{19}$.

Acknowledgments

The authors are grateful to Dr. E. Takayama-Muromachi of NIRIM for his encouragement throughout this study, to Mr. N. Minakawa and Mr. Y. Shimojo for their help with the neutron diffraction experiment, and to the members of the JRR-3 Operation Division, Department of Research Reactor Operation, JAERI.

References

1. W. D. TOWNES, J. H. FANG, AND A. J. PERROTTA, *Z. Kristallogr.* **125,** 437 (1967).
2. V. L. MORUZZI AND M. W. SHAFER, *J. Am. Ceram. Soc.* **43,** 367 (1960).
3. A. AHARONI AND M. SHIEBER, Phys. Rev. **123,** 807 (1961).
4. J. S. VAN WIERINGEN, *Philips Tech. Rev.* **28,** 33 (1967).
5. R. L. STREEVER, *Phys. Rev.* **186,** 285 (1969).
6. F. K. LOTGERING, *J. Phys. Chem. Solids* **35,** 1633 (1974).
7. A. M. VAN DIEPEN AND F. K. LOTGERING, *J. Phys. Chem. Solids* **35,** 1641 (1974).
8. CH. SAUER, U. KÖBLER, AND W. ZINN, *J. Phys. Chem. Solids* **39,** 1197 (1978).
9. F. K. LOTGERING, P. R. LOCHER, AND R. P. VAN STAPELE, *J. Phys. Chem. Solids* **41,** 481 (1980).
10. Y. KANKE, K. KATO, E. TAKAYAMA-MUROMACHI, AND M. ISOBE, *Acta Crystallogr. Sect. C* **48,** 1376 (1992).
11. Y. UCHIDA, Y. KANKE, E. TAKAYAMA-MUROMACHI, AND K. KATO, *J. Phys. Soc. Jpn.* **60,** 2530 (1991).
12. Y. KANKE, F. IZUMI, E. TAKAYAMA-MUROMACHI, K. KATO, T. KAMIYAMA, AND H. ASANO, *J. Solid State Chem.* **92,** 261 (1991).
13. Y. KANKE, E. TAKAYAMA-MUROMACHI, Y. UCHIDA, K. KATO, AND S. TAKEKAWA, *J. Solid State Chem.* **95,** 438 (1991).
14. Y. MORII, K. FUCHIZAKI, S. FUNAHASHI, N. MINAKAWA, Y. SHIMOJYO, AND A. ISHIDA, *in* "Proceedings of the 4th International Symposium on Advanced Nuclear Research, Mito, Japan, February 1992," in press.
15. F. IZUMI, *in* "The Rietveld Method" (R. A. Young, Ed.), Chap. 13, Oxford Univ. Press, Oxford (1993).
16. V. F. SEARS, *in* "Neutron Scattering" (K. Sköld and D. L. Price, Eds.), Methods of Experimental Physics, Vol. 23, Part A, p. 521, Academic Press, New York (1986).
17. X. OBRADORS, A. COLLOMB, M. PERNET, D. SAMARAS, AND J. C. JOUBERT, *J. Solid State Chem.* **56,** 171 (1985).
18. X. OBRADORS, X. SOLANS, A. COLLOMB, D. SAMARAS, J. RODRIGUEZ, M. PERNET, AND M. FONT-ALTABA, *J. Solid State Chem.* **72,** 218 (1988).
19. A. UTSUNOMIYA, K. TANAKA, H. MORIKAWA, F. MARUMO, AND H. KOJIMA, *J. Solid State Chem.* **75,** 197 (1988).
20. N. IYI, S. TAKEKAWA, AND S. KIMURA, *J. Solid State Chem.* **85,** 318 (1990).
21. K. KIMURA, M. OHGAKI, K. TANAKA, H. MORIKAWA, AND F. MARUMO, *J. Solid State Chem.* **87,** 186 (1990).
22. P. B. BRAUN, *Philips Res. Rep.* **12,** 491 (1957).
23. R. D. SHANNON, *Acta Crystallogr. Sect. A* **32,** 751 (1976).
24. M. C. CADÉE AND D. J. W. IJDO, *J. Solid State Chem.* **52,** 302 (1984).
25. M. DROFENIK, D. HANŽEL, DARKO HANŽEL, M. N. DESCHIZEAUX-CHÉRUY, AND J. C. JOUBERT, *J. Solid State Chem.* **79,** 119 (1989).

26. W. C. HAMILTON, *Phys. Rev.* **110,** 1050 (1958).
27. B. REUTER AND E. RIEDEL, *Z. Anorg. Allg. Chem.* **369,** 306 (1969).
28. Y. ISHIKAWA, S. SATO, AND Y. SYONO, *J. Phys. Soc. Jpn.* **31,** 452 (1971).
29. M. ABE, M. KAWACHI, AND S. NOMURA, *J. Phys. Soc. Jpn.* **33,** 1296 (1972).
30. K. KATO, I. KAWADA, N. KIMIZUKA, AND T. KATSURA, *Z. Kristallogr.* **141,** 314 (1975).
31. N. KIMIZUKA AND T. MOHRI, *J. Solid State Chem.* **78,** 98 (1989).
32. W. GONG, J. E. GREEDAN, G. LIU, AND M. BJORGVINSSON, *J. Solid State Chem.* **94,** 213 (1989).
33. J. C. BOULOUX AND J. GALY, *Acta Crystallogr. Sect. B* **29,** 269 (1973).
34. J. C. BOULOUX AND J. GALY, *Acta Crystallogr. Sect. B* **29,** 1335 (1973).
35. X. OBRADORS, A. ISALGUE, A. COLLOMB, A. LABARTA, M. PERNET, J. A. PEREDA, J. TEJADA, AND J. C. JOUBERT, *J. Phys. C* **19,** 6605 (1986).
36. L. E. ORGEL, "An Introduction to Transition–Metal Chemistry Ligand-Field Theory," 2nd ed., Methuen, p. 72 (1966).
37. D. B. ROGERS, J. L. GILLSON, AND T. E. GIER, *Solid State Commun.* **5,** 263 (1967).
38. E. J. W. VERWEY AND P. W. HAAYMAN, *Physica* **8,** 979 (1941).
39. M. IIZUMI, T. F. KOETZLE, G. SHIRANE, S. CHIKAZUMI, M. MATSUI, AND S. TODO, *Acta Crystallogr. Sect. B* **38,** 2121 (1982).